THE JOURNAL OF PHYSICAL CHEMISTRY Letters

Letter

pubs.acs.org/JPCL

# Nanodiamond as a New Hyperpolarizing Agent and Its $^{13}$C MRS

Prasanta Dutta, Gary V. Martinez, and Robert J. Gillies*

Department of Cancer Imaging and Metabolism, H. Lee Moffitt Cancer Center & Research Institute, Tampa, Florida 33612, United States

Supporting Information

**ABSTRACT:** In this work, we have hyperpolarized carbonaceous nanoparticles ($D \approx 10$ nm), that is, "nanodiamonds", with 1.1% $^{13}$C (natural abundance) using dynamic nuclear polarization (DNP). The polarization buildup curve showed a signal enhancement with relative intensity up to 4700 at 1.4 K and 100 mW microwave power. $^{13}$C magnetic resonance spectra (MRS) were obtained from the sample at 7 T, and the signal decayed with a $T_1$ of 55 ± 3s. Notably, polarization was possible in the absence of added radical, consistent with previous results showing endogenous unpaired electrons in natural nanodiamonds. These likely contribute to the shorter $T_1$'s compared to those of highly pure diamond. Despite the relatively short $T_1$, these observations suggest that natural nanodiamonds may be useful for in vivo applications.

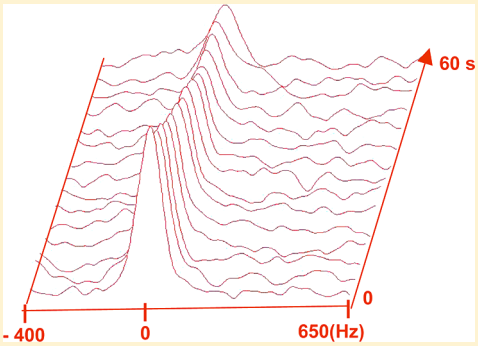


**SECTION:** Physical Processes in Nanomaterials and Nanostructures

In dynamic nuclear polarization (DNP), the large polarization of electron spins is transferred to nuclear spins, enhancing the signal intensities up to $10^3$−$10^4$ for subsequent nuclear magnetic resonance (NMR) spectroscopy and imaging.[1] Once the nuclear polarization builds up inside of the compound, it is stored for a time, on the order of the nuclear $T_1$ (spin−lattice) relaxation time. The DNP methodology in particular is very versatile, and many different molecules have been polarized.[2] The preponderance of in vivo work has been focused on one molecule ($^{13}$C-labeled pyruvate),[3] largely because its relaxation time $T_1$ is relatively long (40−60 s) and it is a central metabolic intermediate that is rapidly converted into numerous visible metabolic products (e.g., lactate, alanine, and bicarbonate).[2] For metabolic studies, the polarized nuclei must undergo metabolic reactions before the signal returns to thermal equilibrium and becomes undetectable. Although this lifetime permits investigation of important metabolic processes, it is vastly shorter than the decay lifetimes associated with radiotracers in molecular imaging, such as $^{18}$F in positron emission tomography (PET), which has a half-life of ∼2 h. Recently developed hyperpolarized $^{13}$C-labeled substrates are being injected to monitor real-time metabolic activity in vivo. Hyperpolarized $^{13}$C MRS and MRI have been applied to measure extracellular $pH_e$ and to study several metabolic pathways and enzymatic activity by enriching different substrates such as pyruvate, fumarate, and bicarbonate with $^{13}$C.[4−6] Because the hyperpolarized magnetization decays with time, substrates with $T_1$ values in excess of 20 s are necessary to image metabolic events, imposing limitations on available probes. Although specific symmetrical chemistries have been developed to maintain spin polarization for extended times, this also has a limited number of potential applications.[7] The choice of an appropriate substrate or agent is influenced by the $T_1$ relaxation time of the hyperpolarized nuclei, the level of polarization, and the rate at which the substrate reaches its target. Besides $^{13}$C-labeled molecules, other substrates with different nuclei including $^{15}$N, $^{89}$Y, and $^{29}$Si have been polarized using DNP to investigate their $T_1$'s and the level of polarization.[8−10]

In this work, we demonstrate hyperpolarization of nanodiamond and acquire its $^{13}$C MR spectra. The particle size of the sample (Sigma-Aldrich) was confirmed by transmission electron microscopy (TEM) (Figure 1A). The diameter of the nearly spherical shaped particle is about 10.0 ± 1.5 nm. The details of the sample preparation for the DNP experiment are provided in the Experimental Methods section. The hyperpolarization buildup was observed and monitored for 3 h with varying microwave powers and temperatures, as shown in Figure 1B and C. The polarization does not vary as much with microwave power as it does with increasing the temperature, which yields a polarization decrease. The highest solid-state buildup or relative intensity that was measured by DNP, using a Hypersense instrument (Oxford Instruments), was about 4700 at 1.4 K and 100 mW of power. We also determined that the solid-state polarization buildup time constant ($T_C$) for this nanodiamond sample was 1120 ± 30s. Using the same DNP conditions, the typical $T_C$ of $^{13}$C-pyruvate is 850 s, and that for $^{13}$C-bicarbonate is 3500 s.[11]

The microwave sweep experiments were performed for both nanodiamond and $^{13}$C-pyruvic acid samples, as shown in Figure 2A. The optimum frequencies determined from the positive

**Received:** December 7, 2013
**Accepted:** January 27, 2014

   dx.doi.org/10.1021/jz402659t | J. Phys. Chem. Lett. 2014, 5, 597−600

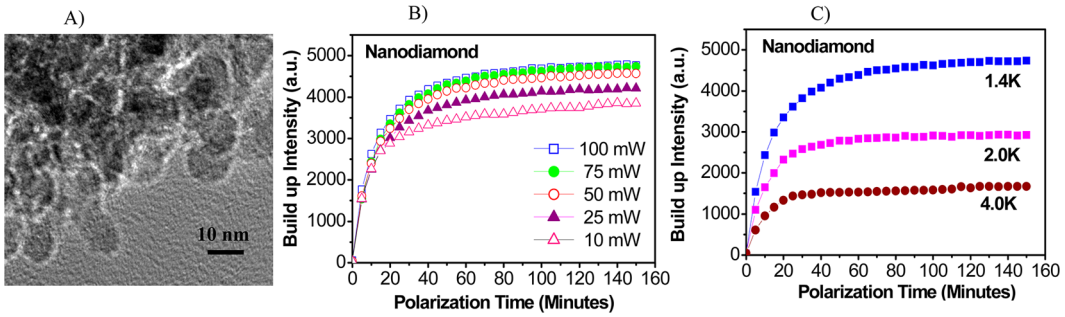


**Figure 1.** (A) Transmission electron micrograph (TEM) of the diamond nanoparticles dispersed in acetone. (B,C) The solid-state polarization buildup curve with polarizing time for different microwave powers at 1.4 K and for several temperatures at 100 mW of power, respectively.

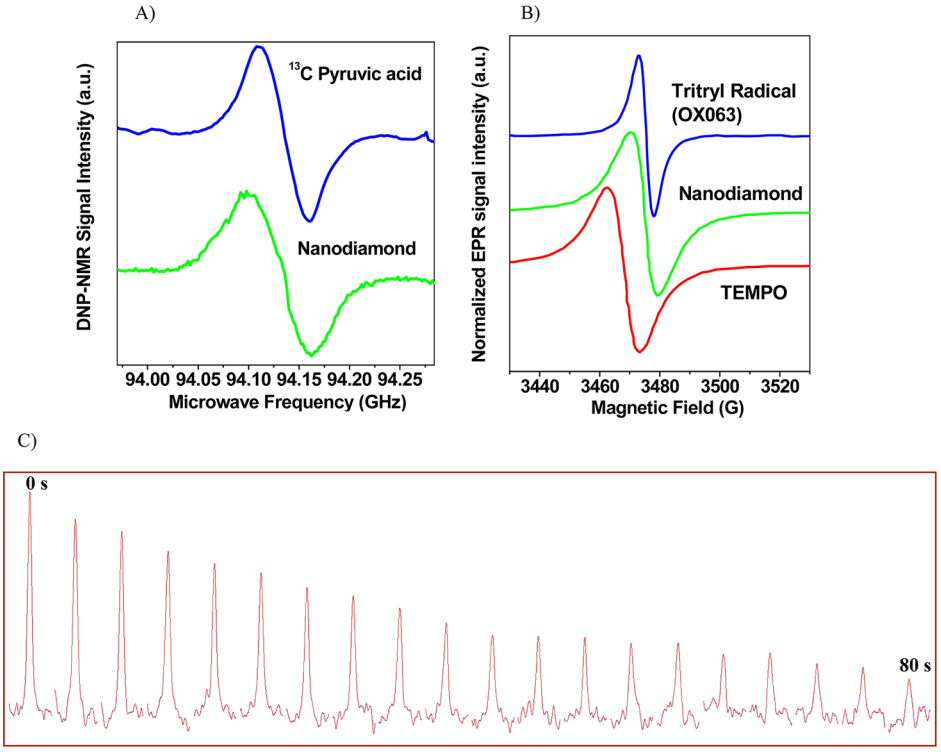


**Figure 2.** (A) Microwave sweep data at 1.4 K for $^{13}$C-pyruvic acid with 15 mM trityl radical (OX063) and nanodiamond samples. (B) Room-temperature X-band EPR spectra of OX063, nanodiamond, and TEMPO, over a sweep width of 100 G. Data were normalized to their peak values. (C) Representative dynamic array (horizontal) of $^{13}$C MRS of hyperpolarized nanodiamond after the dissolution process. A $T_R$ = 4s was employed for this scan.

polarization maximum frequency were 94.098 GHz for nanodiamond and 94.110 GHz for $^{13}$C-pyruvic acid. The separations between the polarization maximum and minimum frequencies were measured as 62 and 50 MHz for nanodiamond and $^{13}$C-pyruvic acid, respectively. Representative room-temperature electron paramagnetic resonance (EPR) spectra for tritryl radical (OX063), nanodiamond, and TEMPO are shown in Figure 2B. The EPR parameters of these samples are listed in Table 1. It is important to note that the resonance fields or $g$ factors for the trityl radical and nanodiamond were exactly the same, although the EPR line width of the nanodiamond is 2-fold higher than that of the trityl radical.

**Table 1. Room-Temperature EPR Parameters for Three Different Samples**

| samples | resonance field (Gauss) | line width (Gauss) | $g$ factor |
|---|---|---|---|
| trityl radical (OX063) | 3475 | 5.0 | 2.0048 |
| nanodiamond | 3475 | 9.5 | 2.0048 |
| TEMPO | 3468 | 10.5 | 2.0089 |

After immediate dissolution, the hyperpolarized sample was placed in a 7 T Agilent ASR scanner to collect the $^{13}$C magnetic resonance spectra. Figure 2C shows an array (horizontal) of spectra that were collected every 4 s ($T_R$) following ~20 s that elapsed during sample transfer. The hyperpolarized signal intensity decayed with time and lasted for more than 150 s (all spectra are not shown here). The line width of the $^{13}$C spectrum was 125 Hz. The $T_1$ value was calculated to be about 55 ± 3s by fitting a theoretical signal equation to the signal intensity (shown in Figure 3A), which is composed of a product of exponential decay functions, $I(T_R) = \cos(\alpha)^{n-1} e^{-(n-1)T_R/T_1}$.[12] These include the effects of spin−lattice relaxation and RF-induced polarization loss. Notably, this DNP hyperpolarization of nanodiamond was achieved without


dx.doi.org/10.1021/jz402659t | J. Phys. Chem. Lett. 2014, 5, 597−600

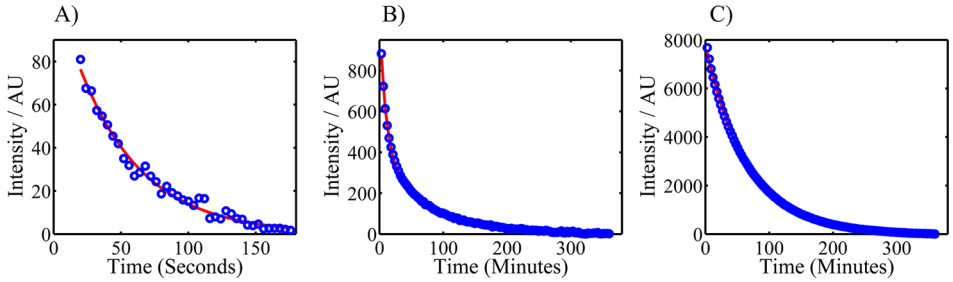


**Figure 3.** (A) Decay of the hyperpolarized $^{13}C$ MRS signal intensity of nanodiamond at room temperature (the theoretical fit estimates $T_1 \approx 55 \pm 3$ s). (B,C) The solid-state $T_1$ measurement data at 1.4 K for nanodiamond and $^{13}C$-pyruvic acid, respectively.

exogenous radicals. It was recently reported that inherent nitrogen vacancies (NVs) in diamond can provide sufficient electron polarization to transfer to $^{13}C$ nuclear polarization.[13] In addition, the unpaired electrons due to dangling bonds of carbon at the nanodiamond's surface may be polarized at low temperature and high magnetic field, which leads to a transfer of electron spin polarization to the $^{13}C$ nuclei.[14]

The spin−lattice relaxation mechanism has been explored in $^{13}C$-enriched bulk diamond sample.[15] $T_1$ relaxations in diamond occur via lattice vibrations that induce transitions in the $^{13}C$ nuclear system via nuclear interactions with an adjacent $^{13}C$ nucleus or trapped paramagnetic atoms or impurities. The $T_1$ can become very long when the interactions between naturally abundant $^{13}C$ nuclei are very weak and the concentration of impurities is low. $^{13}C$-enriched diamonds exhibit a wide range of spin−lattice relaxation times from a few seconds to several hours and even days.[15] The current experiments observed that the $T_1$ value was about 55 ± 3s for these tiny nanodiamond particles after the dissolution process. This relatively short $T_1$ may be due to some structural impurities in the studied nanoparticles, which create paramagnetic centers. The dipolar interaction among these paramagnetic impurities may shorten the $T_1$ relaxation of the diamond nanoparticles. Further, these nanostructures are expected to have shorter correlation times relative to bulk diamond, also leading to decreased $T_1$ values. The solid-state $T_1$'s at 1.4 K of nanodimond and $^{13}C$-pyruvic acid were measured, as shown in Figure 3B and C. The experimental data were well-fitted to a biexponential function, $I_{Bi}(T_R) = m_{0a}e^{-(n-1)T_R/T_{1a}} + m_{0b}\, e^{-(n-1)T_R/T_{1b}}$. The short and long relaxation times of nanodiamond were $T_{1a}$ = 590 ± 11 s and $T_{1b}$ = 4370 ± 42 s, respectively. In contrast, $^{13}C$-pyruvate had a much longer $T_{1a}$ = 2963s ± 625s, with a similar $T_{1b}$ = 4513 ± 443 s. The solid-state $T_1$ values of nanodiamond were more similar to that of silicon nanoparticles, with average values from a recent publication of $T_{1a}$ = 407 s and $T_{1b}$ = 4410 s.[16] The structure of nanodiamond ($D \approx 4.5$ nm) was investigated previously by solid-state NMR spctroscopy.[17] In a recent study, a number of diamond samples of various origin and particle sizes ranging from a few nanometers to micrometers were examined by EPR, solid-state NMR, and DNP techniques.[18] The correlation between particle's size and $^{13}C$ nuclear spin−lattice relaxation times was investigated. The $T_1$ values range from a fraction of a second to several minutes.

Nanodiamonds have the potential to become excellent hyperpolarized contrast agents with sufficiently long $T_1$ times for in vivo uses. Contrast agents with long $T_1$ for hyperpolarized MRI application can be developed using a material whose host substance has no nuclear spin and includes a dopant that has a nonzero nuclear spin. For example, naturally occurring carbon is composed mostly of a $^{12}C$ atom that has zero nuclear spins but also contains spin 1/2 isotopes $^{13}C$ (1.1 wt %). The concentrations of these dipolar spins in a zero-nuclear-spin host can be synthetically optimized by increasing $^{13}C$ labeling. Because the lattice has four directly bonded carbons (Supporting Information), the optimal $^{13}C$ abundance will be between 10 and 20%. This nanodiamond could be as a powder, or the powder can be suspended in a liquid. Particle sizes can be varied from a few nanometers to several micrometers in diameter. In naturally occurring C (diamond), the electronic environment of the nonzero spin component is isotropic, so that weak coupling of electrons to nuclei does not have any preferred orientation. This means that the direction of the nuclear magnetic moment of the nonzero spin component is not locked to the crystal axes of the material or the small particle of material. As a result, even when the individual particles tumble, the nuclear magnetic moment will hold its hyperpolarized orientation. We have estimated that the average number of total carbon atoms is 93 000 in a 10 nm diameter diamond particle, and the average number of $^{13}C$ nuclei (1.1% natural abundance) would be 1023.

Diamond nanoparticles are chemically inert and have no in vivo toxicity. These particles can also be functionalized on the surfaces to cause them to attach to a wide range of specific proteins or cells while maintaining long $T_1$ times. This will allow specific biological surfaces or processes to be tagged by the hyperpolarized nanodiamond for MRI investigation. For example, they can be used to monitor blood circulation in vivo.

In summary, our preliminary experiments have shown that diamond nanoparticles (natural abundance 1.1% $^{13}C$) can be used as hyperpolarizing agents with a considerably longer longitudinal relaxation time ($T_1$) and urge further investigation for using them in in vivo applications.

## EXPERIMENTAL METHODS

*Sample Preparation for DNP Hyperpolarization.* Diamond nanoparticles of size 10 nm were purchased from Sigma-Aldrich (www.sigma-aldrich.com). These nanoparticles were dispersed in a DMSO-$d_6$ (99.9% D, Sigma-Aldrich) and $D_2O$ (1:1 volume) solution. The DMSO and $D_2O$ mixture was used as a glassing agent in this study.

*DNP Hyperpolarization and Dissolution Experiment.* A larger sample cup with 600 μL of the final nanodiamond preparation was placed in the Hypersense hyperpolarizer (Oxford Instrument). The sample was polarized for 3 h at a temperature of 1.4 K and a magnetic field of 3.35 T with microwave irradiation at 94.098 GHz (power = 100 mW). After the polarizations built up and became saturated (as shown in Figure 1B), the sample was collected through the automated dissolution process, as offered by Hypersense. $D_2O$ was used as dissolution media. The


dx.doi.org/10.1021/jz402659t | J. Phys. Chem. Lett. 2014, 5, 597−600

hyperpolarized solution was immediately put into a 7 T magnet (Agilent, ASR) for the $^{13}C$ MRS experiment.

*Microwave Sweep Measurements.* A microwave sweep was performed from 93.970 to 94.284 GHz with a 2 MHz step; each step was polarized for 60 s at 1.4 K and a 100 mW microwave power for both nanodiamond and $^{13}C$-pyruvic acid sample.

*Solid-State Polarization Buildup Measurements.* After determining the optimum microwave frequency from the microwave sweep, the solid-state polarization buildup was measured for different microwave powers and polarization temperatures. The data were collected every 300 s from the NMR spectra using a 90° RF pulse acquire sequence (RINMR software, Oxford Instruments).

*Solid-State $T_1$ Measurements at 1.4 K.* The sample was polarized for 3 h to achieve the maximum polarization at 100 mW of power. Subsequently, the microwave power was turned off, and the NMR signal was collected every 180 s with a RF pulse of a 30° flip angle for 6 h. Nonlinear least-squares regression, using a Levenberg–Marquardt algorithm, was used to fit all relaxation data to a biexponential equation, as described above.

*$^{13}C$ MRS Data Acquisition.* NMR signals for hyperpolarized $^{13}C$ (natural abundance) in diamond nanoparticles were detected using a single RF pulse (SPULS) acquisition sequence with an array of 4 s repetition times ($T_R$). A small flip angle (10°) of the RF pulse was applied to preserve the hyperpolarized signal as long as possible. A double-tuned ($^1H$–$^{13}C$) volume coil was used in this experiment. The $^{13}C$ spin–lattice ($T_1$) relaxation time was determined by performing a monoexponential fit to the signal decay curve of the hyperpolarized sample.

*EPR Measurements.* Room-temperature EPR measurements were performed using a Bruker EMX-220 X-band spectrometer, which operates at a frequency of 9.75 GHz. The peak-to-peak line width ($\Delta H$), resonance magnetic field ($\mathbf{H}_r$), and $g$ factor values were determined for each sample. Bruker's WIN-EPR/SimFonia software was used for processing of EPR spectra.

## ■ ASSOCIATED CONTENT

### Ⓢ Supporting Information

A schematic of the isotopic diamond crystal (Figure S1) and a calculation to estimate the numbers of carbon atoms in a 10 nm diameter diamond particle. This material is available free of charge via the Internet at http://pubs.acs.org.

## ■ AUTHOR INFORMATION

### Corresponding Author

*E-mail: Robert.Gillies@Moffitt.org.

### Notes

The authors declare no competing financial interest.

## ■ ACKNOWLEDGMENTS

The authors gratefully acknowledge the financial support of the Wayne Huizinga Trust and R01 CA077575-14 (R.J.G.). The authors also thank to Professor Mohindar Seehra at West Virginia University and Dr. Stephen Leonard at NIOSH, Morgantown for their help in EPR measurements.

## ■ REFERENCES

(1) Ardenkjaer-Larsen, J. H.; Fridlund, B.; Gram, A.; Hansson, G.; Hansson, L.; Lerche, M. H.; Servin, R.; Thaning, M.; Golman, K. Increase in Signal-to-Noise Ratio of >10,000 Times in Liquid-State NMR. *Proc. Natn. Acad. Sci. USA* **2003**, *100*, 10435–10439.

(2) Dutta, P.; Martinez, G. V.; Gillies, R. J. A New Horizon of DNP Technology: Application to In-Vivo $^{13}C$ Magnetic Resonance Spectroscopy and Imaging. *Biophys. Rev.* **2013**, *5*, 271–281.

(3) Kurhanewicz, J.; Vigneron, D. B.; Brindle, K.; Chekmenev, E. Y.; Comment, A.; Cunningham, C. H.; Deberardinis, R. J.; Green, G. G.; Leach, M. O.; Rajan, S. S.; et al. Analysis of Cancer Metabolism by Imaging Hyperpolarized Nuclei: Prospects for Translation to Clinical Research. *Neoplasia* **2011**, *13*, 81–97.

(4) Dutta, P.; Le, A.; Vander Jagt, D. L.; Tsukamoto, T.; Martinez, G. V.; Dang, C. V.; Gillies, R. J. Evaluation of LDH-A and Glutaminase Inhibition In Vivo by Hyperpolarized $^{13}C$ Pyruvate Magnetic Resonance Spectroscopy of Tumors. *Cancer Res.* **2013**, *73*, 4190–4195.

(5) Gallagher, F. A.; Kettunen, M. I.; Hu, D. E.; Jensen, P. R.; in't Zandt, R.; Karlsson, M.; Gisselsson, A.; Nelson, S. K.; Witney, T. H.; Bohndiek, S. E.; et al. Production of Hyperpolarized [1,4-$^{13}C_2$] Malate from [1,4-$^{13}C_2$] Fumarate is a Marker of Cell Necrosis and Treatment Response in Tumors. *Proc. Natl. Acad. Sci. U.S.A.* **2009**, *106*, 19801–19806.

(6) Gallagher, F. A.; Kettunen, M. I.; Day, S. E.; Hu, D. E.; Ardenkjaer-Larsen, J. H.; in't Zandt, R.; Jensen, P. R.; Karlsson, M.; Golman, K.; Lerche, M. H.; et al. Magnetic Resonance Imaging of pH In Vivo Using Hyperpolarized $^{13}C$-Labelled Bicarbonate. *Nature* **2008**, *453*, 940–944.

(7) Warren, W. S.; Jenista, E.; Branca, R. T.; Chen, X. Increasing Hyperpolarized Spin Lifetimes through True Singlet Eigenstates. *Science* **2009**, *323*, 1711–1714.

(8) Gabellieri, C.; Reynolds, S.; Lavie, A.; Payne, G. S.; Leach, M. O.; Eykyn, T. R. Therapeutic Taget Metabolism Observed Using Hyperpolarized $^{15}N$ Choline. *J. Am. Chem. Soc.* **2008**, *130*, 4598–4599.

(9) Merritt, M. E.; Harrison, C.; Kovacs, Z.; Kshirsagar, P.; Malloy, C. R.; Sherry, A. D. Hyperpolarized $^{89}Y$ Offers the Potential of Direct Imaging of Metal Ions in Biological Systems by Magnetic Resonance. *J. Am. Chem. Soc.* **2007**, *129*, 12942–12943.

(10) Cassidy, M. C.; Chan, H. R.; Ross, B. D.; Bhattacharya, P.; Marcus, C. M. In Vivo Magnetic Resonance Imaging of Hyperpolarized Silicon Particles. *Nat. Nanotechnol.* **2013**, *8*, 363–368.

(11) Wilson, D. M.; Keshari, K. R.; Larson, P. E. Z.; Chen, A. P.; Hu, S.; Van Criekinge, M.; Bok, R.; Nelson, S. J.; Macdonald, J. M.; Vigneron, D. B.; et al. Multi-compound Polarization by DNP Allows Simultaneous Assessment of Multiple Enzymatic Activities In Vivo. *J. Magn. Reson.* **2010**, *205*, 141–147.

(12) Svensson, J.; Mansson, S.; Johansson, E.; Petersson, J. S.; Olsson, L. E. Hyperpolarized $^{13}C$ MR Angiography Using TrueFISP. *Magn. Res. Med* **2003**, *50*, 256–262.

(13) Wang, H. J.; Shin, C. S.; Avalos, C. E.; Seltzer, S. J.; Budker, D.; Pines, A.; Bajaj, V. S. Sensitive Magnetic Control of Ensemble Nuclear Spin Hyperpolarization in Diamond. *Nat. Commun.* **2013**, DOI: 10.1038/ncomms2930.

(14) Manivannan, A.; Chirila, M.; Giles, N. C.; Seehra, M. S. Microstructures, Dangling Bonds and Impurities in Activated Carbons. *Carbon* **1999**, *37*, 1741–1747.

(15) Shabanova, E.; Schaumburg, K.; Sellschop, J. P. F. $^{13}C$ NMR Investigations of Spin–Lattice Relaxation in 99% $^{13}C$ Enriched Diamonds. *J. Magn. Reson.* **1998**, *130*, 8–17.

(16) Atkins, T. M.; Cassidy, M. C.; Lee, M.; Ganguly, S.; Marcus, C. M.; Kauzlarich, S. M. Synthesis of Long $T_1$ Silicon Nanoparticles for $^{29}Si$ Hyperpolarized Magnetic Resonance Imaging. *ACS Nano* **2013**, *7*, 1609–1617.

(17) Fang, X. W.; Mao, J. D.; Levin, E. M.; Schmidt-Rohr, K. Non-Aromatic Core–Shell Structure of Nanodiamond from Solid-State NMR Spectroscopy. *J. Am. Chem. Soc.* **2009**, *131*, 1426–1435.

(18) Casabianca, L. B.; Shames, A. I.; Panich, A. M.; Shenderova, O.; Frydman, L. Factors Affecting DNP NMR in Polycrystalline Diamond Samples. *J. Phys. Chem. C* **2011**, *115*, 19041–19048.